ACS Catalysis

pubs.acs.org/acscatalysis Research Article

The Mechanism of Interfacial CO_2 Activation on Al Doped Cu/ZnO

Maria Heenemann, Marie-Mathilde Millet, Frank Girgsdies, Maik Eichelbaum, Thomas Risse, Robert Schlögl, Travis Jones,* and Elias Frei*

Cite This: ACS Catal. 2020, 10, 5672−5680 Read Online

ACCESS | Metrics & More | Article Recommendations | Supporting Information

ABSTRACT: We report on a combined quantitative charge carrier and catalytic activity analysis of Cu/ZnO(:Al) model catalysts. The promoting effect of Al^{3+} on the ZnO support for CO_2 activation via the reverse water−gas-shift reaction has been investigated. The contact-free and operando microwave Hall Effect technique is applied to measure charge carriers in Cu/ZnO(:Al) based model catalysts under reverse water−gas shift reaction conditions. This method allows us to monitor the electrical conductivity, charge carrier mobility, and absolute number of charge carriers. An increase in charge carrier concentration with increasing Al^{3+} content and its direct correlation with the catalytic activity for CO formation is found. We conclude that the increased availability of charge carriers plays a key role in CO_2 activation and CO formation, which finds additional support in a concurrent decrease of the apparent activation energy and increase in the reaction order of CO_2. In combination with comprehensive DFT calculations, the impact of the interfacial charge transfer, coupled to oxygen defect sites in ZnO and CO_2 adsorption properties, is elucidated and highlighted. In conclusion, the results from this operando investigation combined with DFT calculations demonstrate the importance of charge transfer processes as decisive descriptors for understanding and explaining catalytic properties.

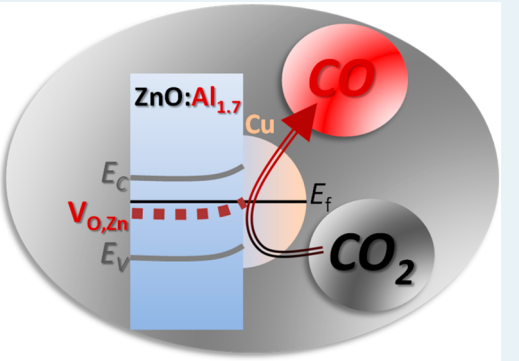

KEYWORDS: *CO_2 activation, Al doped Cu/ZnO, charge carrier quantification, Cu−ZnO interface, rWGS activity*

1. INTRODUCTION

The tremendous quantities of anthropogenic CO_2 that have been released into the atmosphere over the last 200 years have begun to yield noticeable changes to the global climate. Extrapolating into the future, it is clear that continued temperature rise will have dire consequences to life on earth. Strategies are actively being sought to counteract the production of CO_2. One potential route is the conversion of CO_2 into value-added chemicals using energy inputs from renewable resources. This research area is part of the so-called carbon capture and utilization concept for a sustainable future.[1−3] Such processes will necessarily rely on catalysts. One industrial heterogeneous catalyst that is already used for CO_2 activation is the Cu/ZnO/Al_2O_3 system used in methanol production—an important chemical intermediate and alternative fuel—from synthesis gas ($CO/CO_2/H_2$).[4−6] The Cu/ZnO catalyst is also active in the competitive reverse water−gas shift reaction (see eq 1).[7] It is known that the reverse water−gas shift activity over Cu/ZnO-based catalysts is strongly influenced by small amounts of Al added to the oxide support.[8−12] This cationic Al^{3+} dopant acts as a structural and electronic promoter.

$$CO_2 + H_2 \rightleftharpoons CO + H_2O, \quad \Delta H_{298K} = 41.2\ \mathrm{kJ\ mol^{-1}} \tag{1}$$

In general, two different mechanisms have been proposed for the water−gas shift (WGS) and reverse water−gas shift (rWGS) reactions over Cu-based catalysts. First, the formate decomposition and redox cycle have been discussed[13−17] where formate, due to its high stability, is often depicted as a spectator.[18] Second, the commonly assumed surface redox mechanism proposes dissociative CO_2 adsorption as the rate-limiting step.[13,15] Thus, understanding the interaction between the CO_2 molecule and the surface of the catalyst is of fundamental importance. On the basis of theoretical studies, the carbon−oxygen bond is activated by a transfer of electrons from the d-band of the metal into the antibonding orbital of CO_2 to form, e.g., $CO_2^{\delta-}$.[7,19,20] This process is possibly assisted by preadsorbed atomic hydrogen, which accelerates the intermediate formation of, e.g., formates.[21] Since heterogeneous catalysts are often used in a powdered form, the experimental analysis of such charge transfer processes under real operating conditions is challenging. One possible route to gain insight into charge transfer processes would be measuring electrical conductivity, carrier mobility, and charge carrier density. In particular, operando measurements of the

Received: February 3, 2020
Revised: April 18, 2020
Published: April 20, 2020

latter two quantities are, until now, very limited. In situ measurements of the electrical conductivity have been reported,[22] however, a detailed interpretation of the results is hampered by the fact that changes in electrical conductivity may be governed by a change of charge carrier mobility and/or concentration. A strategy to discriminate between these effects is to measure the Hall mobility in addition to the electrical conductivity of the charge carriers.[23] Contact-free electrical conductivity measurements under catalytic relevant conditions have been introduced based on the microwave cavity perturbation technique.[22,24−26] In contrast to that the contact-free Microwave Hall Effect (MHE) allows one to determine not only the electrical conductivity but also carrier mobility changes. Hence, MHE measurements provide access to the charge carrier concentration, the quotient of the electrical conductivity and the Hall mobility (see eq 4, experimental part).[23,27,28] The experimental setup for the MHE measurements utilizes bimodal microwave cavities which exhibit two orthogonal modes and an external static magnetic field perpendicular to the two electrical modes. The principle of the measurement is based on the fact that one of the two modes is excited by an external microwave source while energy is transferred to the orthogonal mode by the Hall effect induced by the charge carriers of a sample inside the bimodal cavitiy. The energy transfer is due to the Lorenz force acting on moving charges excited in the sample by the microwave radiation in the presence of an external static magnetic field and is directly related to the Hall mobility of the charge carriers.[23,27]

Using the above-mentioned MHE method, we have investigated the influence of Al^{3+} dopants on the charge carriers in Cu/ZnO model catalysts under rWGS reaction conditions and characterized the catalytic properties of these systems. A series of Cu/ZnO:Al model catalysts containing different Al^{3+} concentrations were prepared by coprecipitation and subsequent impregnation. Due to a limited solubility of Al^{3+} in ZnO, the highest nominal Al loading was set to 3 mol %. We aim to identify the correlation between the impact of Al^{3+} doping on the rWGS activity and the collective electronic properties of the doped Cu/ZnO model series. The catalyst support and series of model catalysts have been thoroughly characterized by additional techniques like X-ray diffraction (XRD), X-ray fluorescence spectroscopy (XRF), Brunauer−Emmett−Teller surface areas (BET-SA) by N_2-physisorption, for the catalyst supports and model catalysts in a precursor state. The apparent Cu surface area was quantified by N_2O-reactive frontal chromatography (N_2O-RFC). The recently developed operando MHE setup[27] was used for microwave conductivity and Hall mobility measurements at ambient pressure and 230 °C using a $H_2/CO_2/N_2$ feed. For the series of Cu/ZnO:Al model catalysts, additional rWGS experiments at different temperatures and H_2/CO_2 ratios were conducted to obtain the apparent activation energy and reaction order with respect to H_2 and CO_2. Finally, the catalytic data were correlated with the electronic properties and DFT calculations.

2. EXPERIMENTAL SECTION

2.1. Samples. The model catalysts were prepared as described in detail in the Supporting Information(SI). Briefly, ZnO catalyst supports were prepared by pH-controlled coprecipitation.[8,29] The Al^{3+} concentration was varied (nominal 0−3 mol %), and the bare supports were calcined at 330 °C to yield nanocrystalline ZnO. In a subsequent step the samples were impregnated with Cu citrate for a nominal Cu loading of 10 wt %.

2.2. Characterization. All characterization methods aimed at basic properties (XRD, XRF, N_2-physisorption, N_2O-RFC) of the catalysts as well as the rWGS testing unit, are described in the SI.

The newly developed operando MHE setup and the measurement principle will be discussed separately.[27] Prior to the MHE experiment, the samples were reduced in situ for 90 min at 250 °C with a heating rate of 2 °C min^{-1} in the presence of 10 vol % H_2 and 90 vol % He. Afterwards, the temperature was decreased to 230 °C, and the Cu/ZnO:Al catalysts were investigated in 10 vol % H_2/10 vol % CO_2/80 vol % Ar. The CO formation was analyzed online using a micro gas chromatograph (Varian CP-4900, equipped with Por-aPLOT and COX columns). After reaching steady state reactivity, the electronic properties were measured. The effective electrical conductivity, σ, was calculated according to the following equation:[30]

$$\sigma = \pi\varepsilon_0 f_l \left(\frac{Q_e - Q_l}{Q_e Q_l}\right)\frac{1}{\alpha} \tag{2}$$

where ε_0 is the vacuum permittivity, f_l is the resonance frequency of the sample-loaded cavity, Q_e and Q_l are the quality factors of the primary mode of the empty and sample-loaded cavity, respectively. The quality factor is defined as $Q_e = f_e/\Delta f_e$, $Q_l = f_l/\Delta f_l$, where Δf is the frequency width (full width at half-maximum) of the power peak.[22,25] The apparent filling factor, α, depends on the cavity geometry, and was solved numerically. The resultant value is 2.1 V_S/V_C for the TE_{112} cavity used in this setup, where V_S and V_C are the volumes of the sample and cavity, respectively.[27,30] The effective microwave Hall mobility μ_H is defined as follows:

$$\mu_H = K\frac{10^4}{B}\left(\frac{Q_e}{Q_e - Q_l}\right)\left(\frac{E_2(B) - E_2(B=0)}{E_1}\right) \tag{3}$$

where K is the cavity constant, B is the external magnetic flux density (0.6 T), E_1 is the electric field of the incident microwave, and E_2 is the electric field of the transmitted microwave radiation. In case of a perfect resonator it would be sufficient to measure the electric field of the transmitted radiation at the magnetic field of interest only. However, in practice there is always transmitted radiation that is not related to the Hall effect. To remove this effect the transmitted radiation is measured with and without the magnetic field present. The difference between the transmitted electric fields of the these two measurements ($E_2(B) - E_2(B=0) = E_H$) is the part caused by the Hall effect.[28,31,23,27] The factor 10^4 is required if the magnetic flux density B is expressed in Tesla. To improve the sensitivity of the setup a canceling channel was added (see Figure S3). Finally, the charge carrier concentration N_C was obtained from the following:

$$N_C = \frac{\sigma}{\mu_H e} \tag{4}$$

where e is the elementary charge.[23] The averaged values of σ, μ_H, and N_C are given and the error is calculated according to the maximum error of all measured quantities.

https://dx.doi.org/10.1021/acscatal.0c00574
ACS Catal. 2020, 10, 5672−5680

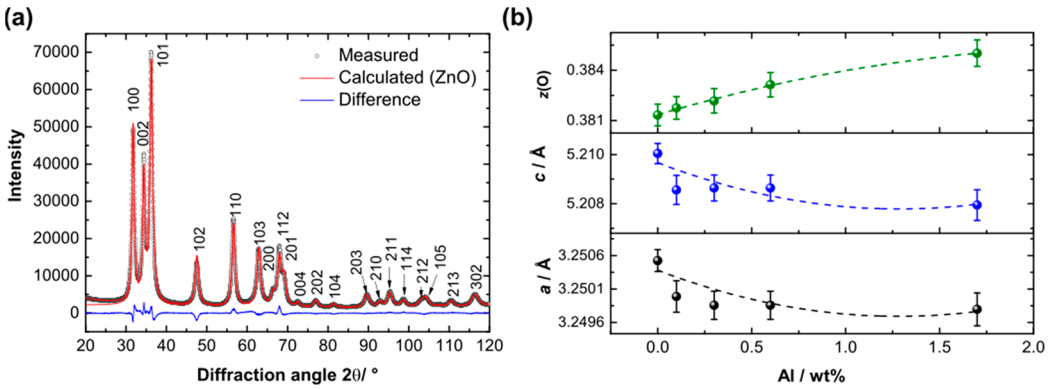

Figure 1. (a) Rietveld fit of ZnO:Al (1.7 wt % Al) with the measured (black circles), calculated (red line) diffraction patterns, the corresponding difference curve (blue line), and (b) Lattice parameters a and c and atomic coordinate *z* of oxygen from the Rietveld refinements as a function of Al content determined by XRF.

3. RESULTS AND DISCUSSION

The focus of this manuscript is to report the influence of Al^{3+} dopants on the absolute charge carrier concentration and its correlation with the catalytic properties of Cu/ZnO model catalysts under rWGS reaction conditions. Prior to the analysis of the electronic properties, the structural ones are thoroughly discussed. If not separately mentioned, then all uncertainties were determined as standard deviations of fitting procedures.

3.1. Sample Characterization. The elemental composition (Al, Zn, and Cu in wt %) of two series of samples, one with Cu (12 wt % CuO) and the other without Cu loading and nominal Al contents ranging from 0 to 3 wt %, were analyzed by XRF and are summarized in Table S1. The measured Al content was found to be lower than the nominal value for all samples, and the difference was larger for the higher nominal contents. In the following, the experimentally determined Al contents are used to identify the samples.

Figure 1a shows a full powder XRD pattern of ZnO:Al (1.7 wt % Al) together with a Rietveld analysis, which is representative for the sample series (Figure S1a). An almost perfect fit of the experimental curves (black circles) by a single phase Rietveld fit of ZnO (red line) with only tiny deviations in the difference curve between theory and experiment (blue line) is observed. For the impregnated and calcined CuO/ZnO:Al a pronounced reflection at $2\theta = 38.6°$ corresponding to CuO(111) is observed as exemplified for the system with an Al content of 1.7 wt % in Figure S2a. For all other diffraction patterns of the CuO/ZnO:Al samples see Figure S1b.

Al is incorporated into the ZnO lattice as evidenced by the contraction of the ZnO unit cell (0.0007 Å for a, 0.002 Å for c) and an increase of the oxygen position along the *z*-axis (z(O) 0.004) with increasing Al content (Figure 1b), caused by the smaller effective ionic radius of Al^{3+} (0.39 Å)[32] than Zn^{2+} (0.6 Å).[32] It is expected that Al occupies the tetrahedral sites in the ZnO wurtzite structure.[8,11,33] In addition, the homogeneous distribution of Al in the ZnO phase increases the coherently scattering domain sizes of ZnO from 11 to 18 nm with decreasing Al content (14−20 nm for impregnated and calcined samples, see Table S2 extracted from Rietveld fitting results). The BET-SA instead increases with increasing Al content from 50 to 84 m^2g^{-1} (Table S1). While the same trend is observed for the series of Cu-loaded samples their BET-SA were found to be consistently smaller, ranging from 34 to 41 m^2g^{-1}. This trend matches perfectly with the domain sizes from the XRD analysis: Within both series of samples crystallite size increases with increasing Al content while the BET-SA decreases (see Tables S1 and S2).

So far, the discussion concerns only the oxidized form of the catalysts. Since the electronic properties and the catalytic data (see below) are gained from the reduced state of the samples, an analysis of the latter state is required. In-situ powder XRD measurements at 250 °C and 5 vol % H_2 in He were conducted to monitor the metallic Cu moieties of the unpromoted Cu/ZnO and the highest promoted Cu/ZnO:Al (1.7 wt % Al). For the unpromoted Cu/ZnO sample, 9.6 ± 0.3 wt % Cu-metal with a domain size of 6.3 nm is measured (extracted from Rietveld fits). The model catalyst with 1.7 wt % Al incorporated into ZnO loaded with 10.6 ± 0.3 wt % Cu-metal shows domain sizes of 5.7 nm (see Table S4). The wt % values for Cu-metal extracted from the in situ XRD data serve for orientation and are absolutely comparable in between the samples and are in reasonable agreement with the XRF values (see Table S1). Although the ZnO domain size decreases as a function of Al-incorporation, the Cu domain size remains almost unaffected. This leads to a better distribution of the Cu particles on the available surface area, without any quantitative adaption on the Cu/ZnO interfacial area. In addition, quantifying the lattice strain of ZnO(:Al), independent of the Cu presence, strain is reduced with Al-doping, meaning that, besides the lattice substitution, some of the intrinsic bulk defects of ZnO are also occupied by Al (Figure S2c). To precisely quantify the redox active surface area after reduction, N_2O-RFC is applied. Surprisingly, the apparent Cu−SA_{N2O} increases with decreasing Al content yielding 5.6 ± 0.3 m^2g^{-1} for the 1.7 wt % Al sample and 6.9 ± 0.4 m^2g^{-1} for the unpromoted Cu/ZnO sample (calculated from the N_2O-capacities, see Table S3). This is explained with the strong metal-support interaction (SMSI) in the Cu/ZnO system. Concomitant to the degree of Al doping, the reducibility of the ZnO increases. This leads to a stronger interaction between metallic Cu and ZnO:Al and to a stronger partial overgrowth (or coverage) of the ZnO:Al support on the Cu particles[8] and thus to a decrease in the Cu−SA_{N2O}.[5,34−38] To quantify the Cu−SA without titrating the, e.g., oxygen vacancies H_2-TPD is used,[39] again for an unpromoted and promoted catalyst (Table S4). The 1.7 wt % Al promoted sample shows a significantly smaller Cu−SA_{H2} of 2.6 ± 0.1 m^2g^{-1} than the unpromoted Cu/ZnO (4.3 ± 0.2 m^2g^{-1}). These results are in line with the lower Cu−SA_{N2O} which already indicated the stronger ZnO_x overgrowth on the Cu particles. As a consequence the coverage

https://dx.doi.org/10.1021/acscatal.0c00574
ACS Catal. 2020, 10, 5672−5680

of Cu sites by partially reduced ZnO_x:Al lead to smaller specific surface areas (N_2O and H_2-TPD) for the promoted catalysts. In summary, the Al incorporation into the ZnO lattice leads to an increase in BET-SA, slightly smaller Cu domain sizes, and a decrease of the available Cu−SA_{N2O}. On the basis of the discussed quantities, with increasing Al doping, the overgrowth induced interfacial contact between Cu and ZnO is optimized at the expense of decreasing available reactive (or metal) surface area.

3.2. Operando Electronic Properties and Corresponding rWGS Activity. Electrical conductivity σ and Hall mobility μ_H were measured during steady state rWGS reaction for the whole series of Al-doped Cu/ZnO catalysts. Prior to these experiments, the samples were reduced and activated (see Methods Section in the SI). The measured electronic effects evidence how charges are transferred as intrinsic materials properties. The electrons are provided by H_2, which is activated on the catalysts surface. With increasing Al content, the electrical conductivity, σ, increases, leading to a doubling for the highest doped sample (1.7 wt % Al in ZnO, Figure 2a). About 0.5 wt % Al doping is already sufficient to reach a significant effect. Concomitantly, the Hall mobility, μ_H, decreases by about 10−15% with increasing Al content. However, the results are interpreted as a general trend, since the rather low value found for the 0.6 wt % Al sample renders a more detailed discussion difficult.

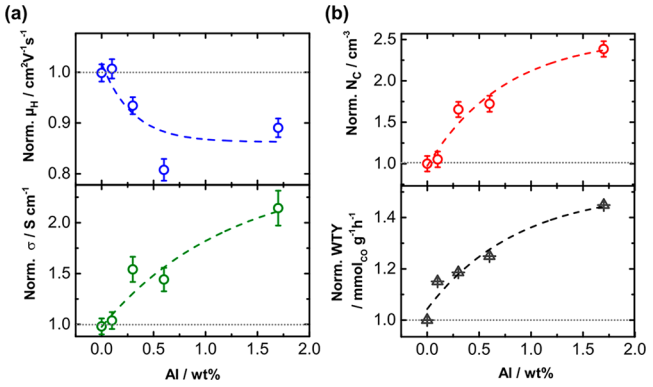

Figure 2. Normalized (to Cu/ZnO) (a) microwave Hall mobility μ_H (blue) and microwave conductivity σ (green) as a function of the Al content which was determined by XRF, and (b) calculated relative charge carrier concentration N_C (red) and weight time yield (WTY) of CO formation under reaction conditions (1 H_2/1 CO_2/8 N_2 at 230 °C).

It is known that electrons are the majority type of charge carriers (n-type semiconductor) in ZnO due to oxygen vacancies and zinc interstitials.[40] The observed contraction of the ZnO lattice parameters by Al doping suggests the incorporation of formally Al^{3+} ions into the ZnO structure. The additional electron is expected to be located in shallow donor states forming close to the conduction band minimum within the ZnO band gap. This corresponds to an n-type doping of the system, which increases the absolute conductivity (free charge carrier density). This interpretation is corroborated by electron paramagnetic resonance studies, which have confirmed the formation of shallow donor states in Al-doped ZnO.[8,41] Since microwaves will penetrate the nanostructured semiconducting material, the measurement is expected to also probe the bulk property (here, given by effective values for the powders).[22,23,42] From these observations, we conclude that Al acts as a strong electron donor in ZnO, resulting in a distinct increase in its bulk conductivity. While the conductivity of the sample increases with increasing Al content, the opposite trend, however, much smaller in size, is observed for the charge carrier mobility. A reduced mobility is directly correlated with a reduction of the mean free path of the electrons or if pictured in the time domain by an increased scattering rate, probably mediated by the increased defect concentration due to the Al doping.[40,43]

As a consequence of the decrease in charge carrier mobility with the amount of dopant, the increased conductivity is explained by an increase of the charge carrier concentration N_C (see eq 4 and Figure 2b). This is perfectly in line with the picture of Al ions donating charges into shallow donor states. The charge carrier concentration N_C increases by a factor of 2.5 (i.e., unpromoted Cu/ZnO vs promoted with 1.7 wt % Al), which means that the conductivity increase clearly overcompensates the reduction in mobility. However, the most important question remains, if the observed change in charge carrier concentration and mobility correlates with the catalytic

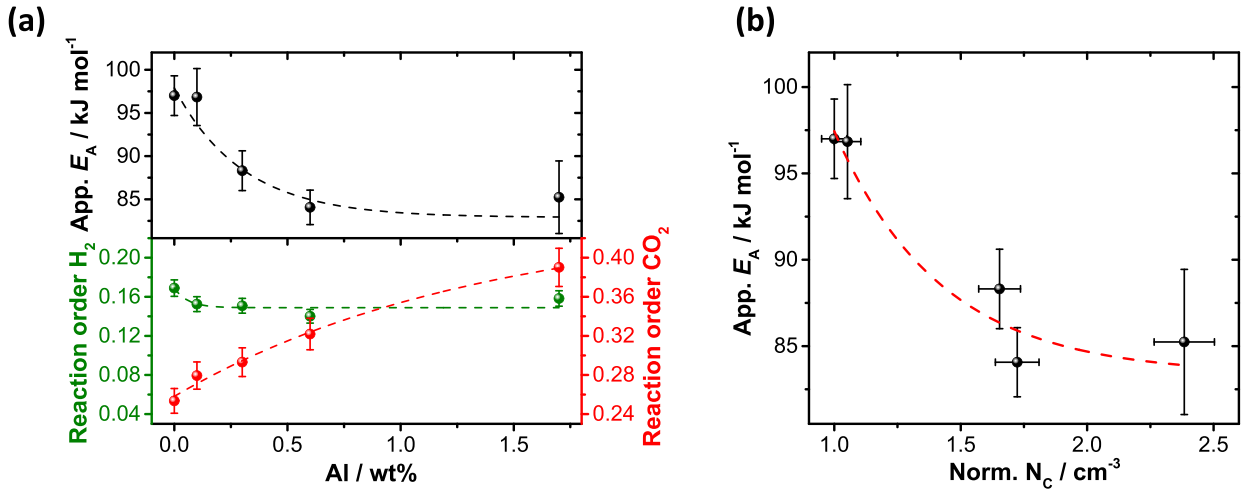

Figure 3. (a) The apparent activation energy of CO formation, the reaction order of H_2 and CO_2 as a function of the Al content, and (b) the apparent activation energy as a function of the relative charge carrier concentration N_C. The dashed lines are drawn to guide the eye.

https://dx.doi.org/10.1021/acscatal.0c00574
ACS Catal. 2020, 10, 5672−5680

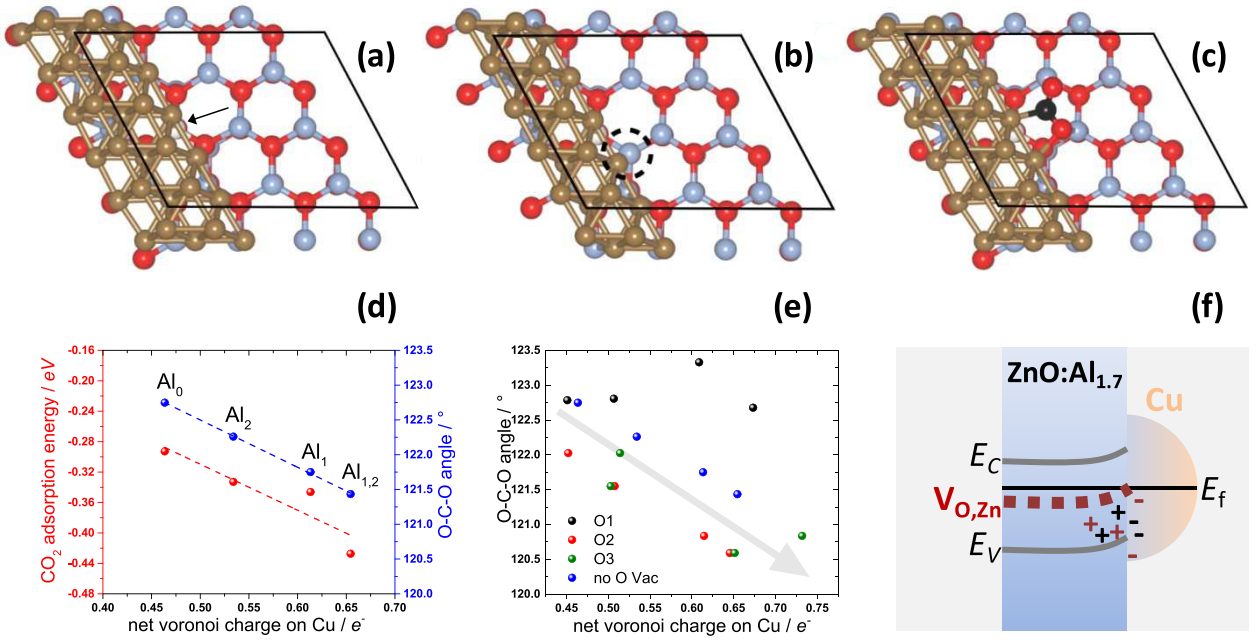

Figure 4. Top view of ZnO ± (0001) slab with a two-layer 20 atom Cu nanostripe (bronze, see also Figure S9). The position of the surface substitutional Al is shown by way of the white sphere (and black arrow), oxygen red and Zn light-blue (a). Example of an oxygen vacancy (black dashed circle) with Al substituent (b). Example of an adsorbed CO_2 molecule (carbon atom, black sphere) at the Cu and ZnO interface with Al substituent (c). Correlation between charge transfer to Cu, the adsorption energy and the interfacial O−C−O angle of adsorbed CO_2 for different Al substituents (Al_0 no substitution, Al_1 for surface, Al_2 for subsurface layer, and $Al_{1,2}$ for double substitution) in the absence of oxygen defects (d). Relationship between the Al induced charge transfer to Cu and the O−C−O angle for all surfaces investigated in this work, where net Voronoi charge is defined as the Voronoi charge relative to neutral Cu (e). Sketch illustrating the charge transfer accumulating at the interface and its origin (red and black, ±) for CO_2 activation over 1.7 wt % promoted Cu/ZnO:Al model catalysts (f). E_C is the conduction band, E_f is the Fermi-level, $V_{O,Zn}$ represent the doping induced vacancies (V_{Zn}'' and $V_O^{\bullet\bullet}$ in Kröger−Vink notation),[58] and E_V is the valence band.

properties of these systems. To this end, CO formation rates were monitored simultaneously (operando) with the aforementioned quantified electronic properties. The lower panel of Figure 2b shows the normalized weight time yield (WTY) of CO as a function of the Al content. Parallel to the increase in conductivity and charge carrier concentration, the WTY of CO also increases with increasing Al doping resulting in about 45% higher WTY for the highly promoted (1.7 wt % Al) as compared to the unpromoted Cu/ZnO catalyst, in line with literature reports.[8,11] Further, the curves of the charge carrier concentration and the CO reaction rates run into a saturation regime, which indicates an effect that works in the opposite direction (decreasing activity). However, these findings provide strong experimental evidence for a direct correlation between the charge carrier concentration and the ability of the system to activate and convert CO_2 as probed by its activity in the rWGS reaction.

3.3. Activity in Reverse Water−Gas Shift Reaction. The catalytic properties of the systems were further elucidated in a tube bundle reactor setup. The linear relationship between the rWGS activity in the MHE setup and the tube bundle reactor shown in Figure S6 further corroborates the applicability of the MHE setup as a catalytic reactor. The catalysts were tested at different temperatures and H_2/CO_2 ratios to obtain the apparent activation energy (app. E_A) and the reaction order of H_2 and CO_2, respectively. Further, the stability of the catalysts under the applied conditions was verified (Figure S7). A decrease of the app. E_A for CO formation with increasing Al content was observed, a drop from 97 ± 3 kJ mol^{-1} for the unpromoted Cu/ZnO to 87 ± 6 kJ mol^{-1} for the 1.7 wt % Al promoted Cu/ZnO (Figure 3a upper panel, for corresponding Arrhenius plots see Figure S5). This trend fits very nicely with the CO WTY determined in the operando MHE experiment, again leading to a kind of saturation effect. This indicates that Al^{3+} influences the nature of the active site for rWGS positively, resulting in a lower activation barrier for the rate-determining step. At this point it is worth noting that H_2-activation, which supplies the electrons within the catalytic cycle, does not seem to be critical since the reaction order of H_2 is almost unaffected by any changes in the Al-concentration in ZnO and found to be 0.15 (Figure 3a, lower panel).

Further, Dutta et al. calculated identical barriers for the activation of CO_2 with and without Al as part of ZnO and identified the transfer of an electron to the adsorbate as key process.[44] This charge transfer, to e.g., the lowest unoccupied $2\pi_u$ antibonding orbital of CO_2,[20] would lead to a bent, anionic CO_2^- species.[7,20,45] The activated, metastable CO_2^- species would then be further transformed into a surface intermediate (e.g., carboxylate, formate or carbonate),[7,46,47] which acts as a precursor to the formation of the product CO. The transformation of the activated CO_2 to a reaction intermediate is a very fast process (short lifetime in the μs-range),[48] rendering its spectroscopic investigation impossible due to the low transient concentration. The reaction order of CO_2 increases from 0.25 to 0.36 with increasing Al content (Figure 3a lower panel and Table S5 of the SI). This trend in the reaction order to higher values means that the $p(CO_2)$ has a stronger influence on the CO rates (higher rate per reaction site) for the highly Al-doped system and that the

https://dx.doi.org/10.1021/acscatal.0c00574
ACS Catal. 2020, 10, 5672−5680

corresponding reaction sites are more available (less covered). These reaction orders agree well with those of similar Cu/ZnO based catalyst studies[8,15,38] and indicate that the critical activation of CO_2 is directly influenced by the degree of Al doping. Figure 3b shows that the apparent activation energies decrease as a function of the relative charge carrier concentration N_C, which in turn highlights the complex role (structural and electronic) of the Al dopant on the active site of the catalyst and the reaction rates in the rWGS. An increased N_C is coupled to a decreased app. E_A leading to an enhanced catalytic activity explained by the intimate interfacial contact of Cu and ZnO moieties steered by Al-dopants.

To understand the effect of doping we can turn to concepts from solid state physics. Schwab reported in the 1960s that the activation energy of a mixed catalyst (metal and support) can be lowered or raised by doping. Depending on the metal, the support and the applied reaction, n- or p-type doping can lead to an enhanced catalytic activity as explained qualitatively within a band model.[49] The Cu/ZnO system represents a metal/semiconductor junction (or Schottky−Mott junction) which forms a Schottky barrier. Frost[50] suggested that electrons are transferred via this junction.[51,52] It is reported, that the Cu/ZnO interface plays an important role as an active catalytic site in rWGS[38] and methanol synthesis,[9,53,54] where oxophilic $Zn^{\delta+}$ sites (present as oxygen deficient $Zn^{\delta+}O_x$) covering Cu particles act as adsorption sites for CO_2.[38,55] It is assumed that the band-bending, as schematically shown in Figure 4f, of the oxide is proportional to the charge transfer. These charges are rather localized at interfacial Cu sites coupled to the corresponding metal states. Beyond this interfacial transfer, the metal conduction electrons efficiently screen the residual metal particle. As a consequence, the manipulation of bulk properties like doping might results in rather local adaptions of the interfacial (electronic) structure and electronic properties.

To shed light on the still debated consequences of the Cu−ZnO(:Al) interface, comprehensive DFT calculations of a Cu nanocluster (or -stripe) on top of Al doped and undoped ZnO were conducted (details to the calculations, see SI). Besides the stability of the Al-dopant as part of the ZnO lattice (see also Figure 1b), the net charge transfer (discussed in the following on the basis of a Voronoi partitioning scheme, see SI for details concerning the determination of the charge transfer) from ZnO to Cu and the CO_2 adsorption on the Cu−ZnO(:Al) interface for different cases of oxygen vacant sites are considered. Experimentally it has been found that reductive conditions lead to an enrichment of Al at the surface of the ZnO.[11,33] To mimic the interface of bulk Cu and ZnO, calculations on a five layer thick Cu film on ZnO(:Al) were performed. Al substitution for Zn in the first subsurface layer is identified as energetically most favorable compared to the surface and the second subsurface layer (Figure S8a−c). Thus, we focused on the impact of Al doping in the surface and the first subsurface layer, respectively.

Figure 4a shows a representative configuration of substitutional Al doping of ZnO at the interface to a Cu nanostripe (Al_1) corresponds 1.04 at% Al in the ZnO cluster. Energetically this configuration is 1.05 eV higher in energy than a substitutional Al doping in the first subsurface layer (Al_2) of ZnO. The net charge transfer is increased by doping the ZnO lattice with Al. An Al atom in the surface layer (Al_1) raises the charge transfer from 0.46 e^- (pure ZnO) to 0.61 e^-, while doping in the first subsurface layer (Al_2) results in a smaller effect of 0.53 e^- (see also Table S6). This points to a direct Cu/Al interaction at the interface, explaining the lower value for subsurface substitution. Double substitution ($Al_{1,2}$, corresponding to 2.08 at% Al doping) leads to the highest charge transfer of 0.65 e^-, which is only slightly smaller than the sum of the individual effects. The results clearly show that Al doping promotes electron transfer from ZnO to Cu metal. The charge accumulates at the interface and results in a decrease of the Cu layer distances near the interface (see Figure S8d,e). The direction of the charge transfer at the interface is also in agreement with the results of Beinik et al.,[56] discussing upward band-bending of ∼0.4 eV. Besides, even under industrially relevant conditions, oxygen deficient ZnO transfers charge to form $Au^{\delta-}$.[57]

For a realistic description of the material, besides the electronic impact, the situation with respect to defects must also be considered.[8,11,39] Figure 4b shows, as example, one kind of oxygen vacant site near the Al dopant (see also Figure S10a−c, different oxygen vacancies O1, O2, and O3). Varying the level and position of Al doping as well as the presence and location of oxygen vacancies at the Cu/ZnO(:Al) interface, allows one to calculate a set of adsorption energies and O−C−O bond angles of CO_2 (for adsorption sites, Figure 4c); the O−C−O bond angle is a sensitive probe for the degree of charge transfer onto CO_2, hence, its activation and the catalytic performance. Figure 4d shows the adsorption energy and the O−C−O angle of adsorbed CO_2 as a function of the Al induced charge transfer towards Cu (here: no oxygen vacancies are considered). In these cases, both the CO_2 adsorption energy, and perhaps more importantly, the O−C−O bond angle scale linearly with the number of transferred electrons as the only change to the system is the degree of charge transfer to the metal. The decreased bond angle indicates adsorbed CO_2 activation increases with charge transfer to Cu, which is crucial for its catalytic transformation.

While the preceding examples demonstrate Al doping alone can strengthen CO_2 adsorption by about 0.15 eV (see Figure 4d and Table S6). The effect of anionic defects depends on their location, and hence interaction with the adsorbate (Figure S11a−c). In case the CO_2 molecule is located close to the empty anionic lattice site and can interact with it directly (O1 and O2 vacancy, Figure S11), a drop of 0.24 eV (O1 vacancy, Figure S11a,d), or an increase of 0.12 eV (O2 vacancy, Figure S11b,d) in adsorption energy were found. However, when the vacancy cannot directly interact with the interfacial CO_2 adsorbate (O3, Figure S11c,d), its effect on the adsorption energy is negligible. Combining the effect of Al doping and O vacancy formation, CO_2 adsorption energy (plotted as a function of the Al induced charge transfer to the interfacial Cu, Figure S12) is strongly correlated with the position of O vacancy. The adsorption energy decreases with increasing level of charge transfer onto the Cu particles in case the adsorbing CO_2 can interact directly with the oxygen vacancy (O1 and O2 positions). If no direct interaction can occur (O3 position) as also found for the vacancy free ZnO, the adsorption energy increases with the level of charge transfer (Figure 4d). In summary, the CO_2 adsorption energy is more strongly coupled to oxygen defects than to charge transfer, which evidence the structural impact of the Al-dopant (see Figure S12). However, CO_2 activation, as seen by way of the O−C−O angle, is still mediated by oxide to metal charge transfer, the trend remains more consistent than that found for adsorption energy, see Figure 4e. The oxide to metal charge

https://dx.doi.org/10.1021/acscatal.0c00574
ACS Catal. 2020, 10, 5672−5680

transfer induced by Al doping tends to lead to an increased activation of CO_2 for any O vacancy position, though the destabilizing O1 vacancy still remains somewhat of an outlier (black spheres in Figure 4e). Here the electronic influence of Al as a dopant becomes visible as crucial for the CO_2 activation. Our findings are schematically summarized in Figure 4f, which serves as suitable connection between the experimental results discussed above and the DFT calculations on the state of the complex Cu/ZnO(:Al) interfacial contact. The intrinsic n-type semiconductor ZnO donates electrons, leading to negatively charged Cu metal nanoparticles, while the differently Al^{3+} doped ZnO supports control the quantity of charge transfer. The incorporation of Al^{3+} in ZnO leads to a different defect distribution in the support (and at the interface to Cu),[39] indicated as $V_{O,Zn}$ (or generally as additional shallow donor states near the conduction band).[8,56] Besides, the increase in the reducibility of ZnO due to the incorporation of Al^{3+} leads to partially covered Cu particles (lower $Cu-SA_{N2O}$)[9,10] and a larger Cu/ZnO:Al interface. As a consequence, the higher Al-doped samples provide more free charge carriers for the activation (smaller O−C−O angles) and conversion of CO_2, respectively, as critical step of the rWGS reaction (decrease in app. E_A).

4. CONCLUSIONS

Operando techniques aim to provide insights into the working state of catalysts. A series of Al-doped Cu/ZnO model catalysts was investigated, simultaneously measuring their catalytic activity and electronic properties. The measurements reveal a direct correlation between the free charge carrier concentration and the activity in the rWGS reaction. The availability of free charge carriers is steered by the amount of the Al^{3+} doping as part of the ZnO lattice. DFT calculations demonstrate the direction of the charge transfer is from ZnO:Al metal oxide toward the Cu metal particles. The charge accumulation at the interface of the Cu/ZnO:Al contact decreases the Cu interlayer distances. Beyond this, a correlation of the charge transfer and the O−C−O bond angle is identified with CO_2 activation. This is directly mirrored in a decrease of the E_A and increased reaction order of CO_2. Since electronic and structural effects are coupled phenomena (Al changes the crystal structure, reducibility, defect density and electronic structure), oxygen vacancies can have a crucial influence on the stabilization and activation of adsorbed CO_2 species.

In summary, the combined operando-DFT-study on Al doped Cu/ZnO catalysts clarify the so far controversially discussed role of the Cu/ZnO:Al interface as complex reaction site for the CO_2 activation and conversion, where numerous structural and electronic adaptions define the catalytic performance. These findings are added to the important contributions of Cu defects,[5] the mechanistic role of interfacial Zn−OH groups[53,55] and the surface enrichment of ZnO[59] (predetermining the product selectivity of CO_2 hydrogenation toward CO, highly enriched,[38] or CH_3OH, moderately enriched[60]). The process of CO_2 activation and conversion at the Cu/ZnO interface seems to be unraveled as an example of perfect synergism.

ASSOCIATED CONTENT

Supporting Information

The Supporting Information is available free of charge at https://pubs.acs.org/doi/10.1021/acscatal.0c00574.

Detailed descriptions on the synthesis of the samples; characterization methods like XRF, XRD, and catalytic testing; and additional details to the DFT calculations are shown (PDF)

AUTHOR INFORMATION

Corresponding Authors

Travis Jones − *Fritz-Haber-Institut der Max-Planck-Gesellschaft, Department of Inorganic Chemistry, 14195 Berlin, Germany;* orcid.org/0000-0001-8921-7641; Email: trjones@fhi-berlin.mpg.de

Elias Frei − *Fritz-Haber-Institut der Max-Planck-Gesellschaft, Department of Inorganic Chemistry, 14195 Berlin, Germany;* orcid.org/0000-0003-3565-1199; Email: efrei@fhi-berlin.mpg.de

Authors

Maria Heenemann − *Fritz-Haber-Institut der Max-Planck-Gesellschaft, Department of Inorganic Chemistry, 14195 Berlin, Germany*

Marie-Mathilde Millet − *Fritz-Haber-Institut der Max-Planck-Gesellschaft, Department of Inorganic Chemistry, 14195 Berlin, Germany*

Frank Girgsdies − *Fritz-Haber-Institut der Max-Planck-Gesellschaft, Department of Inorganic Chemistry, 14195 Berlin, Germany*

Maik Eichelbaum − *Technische Hochschule Nürnberg Georg Simon Ohm, Faculty of Applied Chemistry, Institute of Analytical Chemistry, 90489 Nürnberg, Germany*

Thomas Risse − *Freie Universität Berlin, Institute of Chemistry and Biochemistry, 14195 Berlin, Germany*

Robert Schlögl − *Fritz-Haber-Institut der Max-Planck-Gesellschaft, Department of Inorganic Chemistry, 14195 Berlin, Germany; Max Planck Institute for Chemical Energy Conversion, Heterogeneous Reactions, 45470 Mülheim an der Ruhr, Germany*

Complete contact information is available at: https://pubs.acs.org/10.1021/acscatal.0c00574

Notes

The authors declare no competing financial interest.

ACKNOWLEDGMENTS

The authors address special thanks to the late Prof. R. Stößer, and Prof. K.-P. Dinse for development of the bimodal microwave Hall effect system. We thank Dr. O. Timpe for XRF analysis, J. Plagemann for BET analysis and E. H. Wolf for help with the rWGS activity measurements. The study was funded in part by the Deutsche Forschungsgesellschaft (EI 950/1-1,2). M.H. thanks the IMPRS (Functional Interfaces in Physics and Chemistry) for financial support. T.J. thanks Höchstleistungsrechenzentrum Stuttgart (HLRS) for access to the supercomputer HazelHen.

REFERENCES

(1) Karl, T. R.; Trenberth, K. E. Modern global climate change. *Science* **2003**, *302*, 1719−1723.

(2) Lim, X. How to make the most of carbon dioxide. *Nature* **2015**, *526*, 628.

(3) Quadrelli, E. A.; Centi, G.; Duplan, J. L.; Perathoner, S. Carbon Dioxide Recycling: Emerging Large-Scale Technologies with Industrial Potential. *ChemSusChem* **2011**, *4*, 1194−1215.

(4) Chinchen, G.; Denny, P.; Jennings, J.; Spencer, M.; Waugh, K. Synthesis of methanol: part 1. Catalysts and kinetics. *Appl. Catal.* **1988**, *36*, 1−65.
(5) Behrens, M.; Studt, F.; Kasatkin, I.; Kuehl, S.; Haevecker, M.; Abild-Pedersen, F.; Zander, S.; Girgsdies, F.; Kurr, P.; Kniep, B.-L.; Tovar, M.; Fischer, R. W.; Norskov, J. K.; Schlögl, R. The Active Site of Methanol Synthesis over Cu/ZnO/Al2O3 Industrial Catalysts. *Science* **2012**, *336*, 893−897.
(6) Behrens, M. Promoting the Synthesis of Methanol: Understanding the Requirements for an Industrial Catalyst for the Conversion of CO2. *Angew. Chem., Int. Ed.* **2016**, *55*, 14906−14908.
(7) Freund, H.-J.; Roberts, M. W. Surface chemistry of carbon dioxide. *Surf. Sci. Rep.* **1996**, *25*, 225−273.
(8) Schumann, J.; Eichelbaum, M.; Lunkenbein, T.; Thomas, N.; Alvarez Galvan, M. C.; Schlogl, R.; Behrens, M. Promoting strong metal support interaction: Doping ZnO for enhanced activity of Cu/ZnO: M (M= Al, Ga, Mg) catalysts. *ACS Catal.* **2015**, *5*, 3260−3270.
(9) Lunkenbein, T.; Girgsdies, F.; Kandemir, T.; Thomas, N.; Behrens, M.; Schlögl, R.; Frei, E. Bridging the Time Gap: A Copper/Zinc Oxide/Aluminum Oxide Catalyst for Methanol Synthesis Studied under Industrially Relevant Conditions and Time Scales. *Angew. Chem.* **2016**, *128*, 12900−12904.
(10) Lunkenbein, T.; Schumann, J.; Behrens, M.; Schlögl, R.; Willinger, M. G. Formation of a ZnO Overlayer in Industrial Cu/ZnO/Al2O3 Catalysts Induced by Strong Metal−Support Interactions. *Angew. Chem., Int. Ed.* **2015**, *54*, 4544−4548.
(11) Behrens, M.; Lolli, G.; Muratova, N.; Kasatkin, I.; Havecker, M.; d'Alnoncourt, R. N.; Storcheva, O.; Kohler, K.; Muhler, M.; Schlogl, R. The effect of Al-doping on ZnO nanoparticles applied as catalyst support. *Phys. Chem. Chem. Phys.* **2013**, *15*, 1374−1381.
(12) Kurtz, M.; Bauer, N.; Buscher, C.; Wilmer, H.; Hinrichsen, O.; Becker, R.; Rabe, S.; Merz, K.; Driess, M.; Fischer, R. A.; et al. New synthetic routes to more active Cu/ZnO catalysts used for methanol synthesis. *Catal. Lett.* **2004**, *92*, 49−52.
(13) Ernst, K.-H.; Campbell, C. T.; Moretti, G. Kinetics of the reverse water-gas shift reaction over Cu (110). *J. Catal.* **1992**, *134*, 66−74.
(14) Fujita, S.-I.; Usui, M.; Takezawa, N. Mechanism of the reverse water gas shift reaction over Cu/ZnO catalyst. *J. Catal.* **1992**, *134*, 220−225.
(15) Ginés, M.; Marchi, A.; Apesteguia, C. Kinetic study of the reverse water-gas shift reaction over CuO/ZnO/Al2O3 catalysts. *Appl. Catal., A* **1997**, *154*, 155−171.
(16) Salmi, T.; Hakkarainen, R. Kinetic study of the low-temperature water-gas shift reaction over a Cu—ZnO catalyst. *Appl. Catal.* **1989**, *49*, 285−306.
(17) Grenoble, D.; Estadt, M.; Ollis, D. The chemistry and catalysis of the water gas shift reaction: 1. The kinetics over supported metal catalysts. *J. Catal.* **1981**, *67*, 90−102.
(18) Yang, Y.; Mims, C. A.; Mei, D.; Peden, C. H.; Campbell, C. T. Mechanistic studies of methanol synthesis over Cu from CO/CO 2/H 2/H 2 O mixtures: the source of C in methanol and the role of water. *J. Catal.* **2013**, *298*, 10−17.
(19) Wang, S.-G.; Cao, D.-B.; Li, Y.-W.; Wang, J.; Jiao, H. Chemisorption of CO2 on nickel surfaces. *J. Phys. Chem. B* **2005**, *109*, 18956−18963.
(20) Ko, J.; Kim, B.-K.; Han, J. W. Density Functional Theory Study for Catalytic Activation and Dissociation of CO2 on Bimetallic Alloy Surfaces. *J. Phys. Chem. C* **2016**, *120*, 3438−3447.
(21) Yang, Y.; Evans, J.; Rodriguez, J. A.; White, M. G.; Liu, P. Fundamental studies of methanol synthesis from CO2 hydrogenation on Cu(111), Cu clusters, and Cu/ZnO(0001) with combining macron]). *Phys. Chem. Chem. Phys.* **2010**, *12*, 9909−9917.
(22) Eichelbaum, M.; Stößer, R.; Karpov, A.; Dobner, C. K.; Rosowski, F.; Trunschke, A.; Schlögl, R. The microwave cavity perturbation technique for contact-free and in situ electrical conductivity measurements in catalysis and materials science. *Phys. Chem. Chem. Phys.* **2012**, *14*, 1302−1312.
(23) Chen, L.; Ong, C.; Neo, C.; Varadan, V.; Varadan, V. Microwave theory and techniques for materials characterization. *Microwave Electronics: Measurement and Materials Characterization* **2004**, 37−141.
(24) Eichelbaum, M.; Hävecker, M.; Heine, C.; Karpov, A.; Dobner, C.-K.; Rosowski, F.; Trunschke, A.; Schlögl, R. The Intimate Relationship between Bulk Electronic Conductivity and Selectivity in the Catalytic Oxidation of n-Butane. *Angew. Chem., Int. Ed.* **2012**, *51*, 6246−6250.
(25) Heine, C.; Hävecker, M.; Sanchez-Sanchez, M.; Trunschke, A.; Schlögl, R.; Eichelbaum, M. Work Function, Band Bending, and Microwave Conductivity Studies on the Selective Alkane Oxidation Catalyst MoVTeNb Oxide (Orthorhombic M1 Phase) under Operation Conditions. *J. Phys. Chem. C* **2013**, *117*, 26988−26997.
(26) Eichelbaum, M.; Glaum, R.; Havecker, M.; Wittich, K.; Heine, C.; Schwarz, H.; Dobner, C.-K.; Welker-Nieuwoudt, C.; Trunschke, A.; Schlogl, R. Towards Physical Descriptors of Active and Selective Catalysts for the Oxidation of n-Butane to Maleic Anhydride. *ChemCatChem* **2013**, *5*, 2318−2329.
(27) Heenemann, M. G. M.; Risse, T.; Stößer, R.; Schlögl, R.; Eichelbaum, M.Design of a microwave Hall effect setup for studying in-situ electrical properties of powder catalysts2020, submitted.
(28) Na, B.-K.; Kelly, S.; Vannice, M.; Walters, A. B. Development of the microwave Hall effect technique using an ESR spectrometer and a network analyser. *Meas. Sci. Technol.* **1991**, *2*, 770.
(29) Behrens, M. Meso-and nano-structuring of industrial Cu/ZnO/(Al 2 O 3) catalysts. *J. Catal.* **2009**, *267*, 24−29.
(30) Liu, C.-C.; Na, B.-K.; Walters, A. B.; Vannice, M. A. Microwave absorption measurements of the electrical conductivity of small particles. *Catal. Lett.* **1994**, *26*, 9−24.
(31) Trukhan, E. SHF Apparatus for Measuring Small Losses and Hall Effect. *Instruments and Experimental Techniques-USSR***1965**, *947*.
(32) Shannon, R. t. Revised effective ionic radii and systematic studies of interatomic distances in halides and chalcogenides. *Acta Crystallogr., Sect. A: Cryst. Phys., Diffr., Theor. Gen. Crystallogr.* **1976**, *32*, 751−767.
(33) Frei, E.; Gaur, A.; Lichtenberg, H.; Heine, C.; Friedrich, M.; Greiner, M.; Lunkenbein, T.; Grunwaldt, J.-D.; Schlögl, R. Activating a Cu/ZnO: Al Catalyst − Much More than Reduction: Decomposition, Self-Doping and Polymorphism. *ChemCatChem* **2019**, *11*, 1587−1592.
(34) Grunwaldt, J.-D.; Molenbroek, A.; Topsøe, N.-Y.; Topsøe, H.; Clausen, B. In situ investigations of structural changes in Cu/ZnO catalysts. *J. Catal.* **2000**, *194*, 452−460.
(35) d'Alnoncourt, R. N.; Xia, X.; Strunk, J.; Loffler, E.; Hinrichsen, O.; Muhler, M. The influence of strongly reducing conditions on strong metal−support interactions in Cu/ZnO catalysts used for methanol synthesis. *Phys. Chem. Chem. Phys.* **2006**, *8*, 1525−1538.
(36) Polarz, S.; Strunk, J.; Ischenko, V.; van den Berg, M. W. E.; Hinrichsen, O.; Muhler, M.; Driess, M. On the role of oxygen defects in the catalytic performance of zinc oxide. *Angew. Chem., Int. Ed.* **2006**, *45*, 2965−2969.
(37) Kurtz, M.; Strunk, J.; Hinrichsen, O.; Muhler, M.; Fink, K.; Meyer, B.; Wöll, C. Active Sites on Oxide Surfaces: ZnO-Catalyzed Synthesis of Methanol from CO and H2. *Angew. Chem., Int. Ed.* **2005**, *44*, 2790−2794.
(38) Galván, C. Á.; Schumann, J.; Behrens, M.; Garcio-Fierro, J.-L.; Schlögl, R.; Frei, E. Reverse water-gas shift reaction at the Cu/ZnO interface: Influence of the Cu/Zn ratio on structure-activity correlations. *Appl. Catal., B* **2016**, *195*, 104−111.
(39) Fichtl, M. B.; Schumann, J.; Kasatkin, I.; Jacobsen, N.; Behrens, M.; Schlögl, R.; Muhler, M.; Hinrichsen, O. Counting of oxygen defects versus metal surface sites in methanol synthesis catalysts by different probe molecules. *Angew. Chem., Int. Ed.* **2014**, *53*, 7043−7047.
(40) Özgür, Ü.; Alivov, Y. I.; Liu, C.; Teke, A.; Reshchikov, M. A.; Dogan, S.; Avrutin, V.; Cho, S.-J.; Morkoc, H. A comprehensive review of ZnO materials and devices. *J. Appl. Phys.* **2005**, *98*, 041301.

https://dx.doi.org/10.1021/acscatal.0c00574
ACS Catal. 2020, 10, 5672−5680

(41) Orlinskii, S. B.; Schmidt, J.; Baranov, P. G.; Lorrmann, V.; Riedel, I.; Rauh, D.; Dyakonov, V. Identification of shallow Al donors in Al-doped ZnO nanocrystals: EPR and ENDOR spectroscopy. *Phys. Rev. B: Condens. Matter Mater. Phys.* **2008**, *77*, 115334.
(42) Na, B.-K.; Vannice, M. A.; Walters, A. B. Measurement of the effect of pretreatment and adsorption on the electrical properties of ZnO powders using a microwave-Hall-effect technique. *Phys. Rev. B: Condens. Matter Mater. Phys.* **1992**, *46*, 12266.
(43) Morkoc, H.; Özgür, Ü. *Zinc Oxide Fundamentals, Materials and Device Technology*; WILEY-VCH Verlag GmbH & Co. KGaA, 2008.
(44) Dutta, G.; Sokol, A. A.; Catlow, C. R. A.; Keal, T. W.; Sherwood, P. Activation of carbon dioxide over zinc oxide by localised electrons. *ChemPhysChem* **2012**, *13*, 3453−3456.
(45) Wang, Y.; Kovacik, R.; Meyer, B.; Kotsis, K.; Stodt, D.; Staemmler, V.; Qiu, H.; Träger, F.; Langenberg, D.; Muhler, M.; Wöll, C. CO2 activation by ZnO through the formation of an unusual tridentate surface carbonate. *Angew. Chem., Int. Ed.* **2007**, *46*, 5624−5627.
(46) Grabow, L. C.; Mavrikakis, M. Mechanism of Methanol Synthesis on Cu through CO2 and CO Hydrogenation. *ACS Catal.* **2011**, *1*, 365−384.
(47) Zhao, Y.-F.; Yang, Y.; Mims, C.; Peden, C. H. F.; Li, J.; Mei, D. Insight into methanol synthesis from CO2 hydrogenation on Cu(111): Complex reaction network and the effects of H2O. *J. Catal.* **2011**, *281*, 199−211.
(48) Compton, R. N.; Reinhardt, P. W.; Cooper, C. D. Collisional ionization of Na, K, and Cs by CO2, COS, and CS2: Molecular electron affinities. *J. Chem. Phys.* **1975**, *63*, 3821−3827.
(49) Schwab, G. M. Boundary-Layer Catalysis. *Angew. Chem., Int. Ed. Engl.* **1967**, *6*, 375−375.
(50) Frost, J. Junction effect interactions in methanol synthesis catalysts. *Nature* **1988**, *334*, 577−580.
(51) Yoshihara, J.; Campbell, J.; Campbell, C. Cu films on a Zn-terminated ZnO (0001) surface: structure and electronic properties. *Surf. Sci.* **1998**, *406*, 235−245.
(52) Sheini, F. J.; Singh, J.; Srivasatva, O.; Joag, D. S.; More, M. A. Electrochemical synthesis of Cu/ZnO nanocomposite films and their efficient field emission behaviour. *Appl. Surf. Sci.* **2010**, *256*, 2110−2114.
(53) Kattel, S.; Ramírez, P. J.; Chen, J. G.; Rodriguez, J. A.; Liu, P. Active sites for CO2 hydrogenation to methanol on Cu/ZnO catalysts. *Science* **2017**, *355*, 1296−1299.
(54) Palomino, R. M.; Ramirez, P. J.; Liu, Z.; Hamlyn, R.; Waluyo, I.; Mahapatra, M.; Orozco, I.; Hunt, A.; Simonovis, J. P.; Senanayake, S. D.; Rodriguez, J. A. Hydrogenation of CO2 on ZnO/Cu(100) and ZnO/Cu(111) Catalysts: Role of Copper Structure and Metal−Oxide Interface in Methanol Synthesis. *J. Phys. Chem. B* **2018**, *122*, 794−800.
(55) Tarasov, A. V.; Seitz, F.; Schlögl, R.; Frei, E. In Situ Quantification of Reaction Adsorbates in Low-Temperature Methanol Synthesis on a High-Performance Cu/ZnO:Al Catalyst. *ACS Catal.* **2019**, *9*, 5537−5544.
(56) Beinik, I.; Hellström, M.; Jensen, T. N.; Broqvist, P.; Lauritsen, J. V. Enhanced wetting of Cu on ZnO by migration of subsurface oxygen vacancies. *Nat. Commun.* **2015**, *6*, 8845.
(57) Abdel-Mageed, A. M.; Klyushin, A.; Rezvani, A.; Knop-Gericke, A.; Schlögl, R.; Behm, R. J. Negative Charging of Au Nanoparticles during Methanol Synthesis from CO2/H2 on a Au/ZnO Catalyst: Insights from Operando IR and Near-Ambient-Pressure XPS and XAS Measurements. *Angew. Chem., Int. Ed.* **2019**, *58*, 10325−10329.
(58) Kroger, F. A.; Vink, H. J. Relations between the Concentrations of Imperfections in Crystalline Solids. *Solid State Phys.* **1956**, *3*, 307−435.
(59) Schumann, J.; Lunkenbein, T.; Tarasov, A.; Thomas, N.; Schlögl, R.; Behrens, M. Synthesis and Characterisation of a Highly Active Cu/ZnO:Al Catalyst. *ChemCatChem* **2014**, *6*, 2889−2897.
(60) Zwiener, L.; Girgsdies, F.; Brennecke, D.; Teschner, D.; Machoke, A. G. F.; Schlögl, R.; Frei, E. Evolution of zincian malachite synthesis by low temperature co-precipitation and its catalytic impact on the methanol synthesis. *Appl. Catal., B* **2019**, *249*, 218−226.

https://dx.doi.org/10.1021/acscatal.0c00574
ACS Catal. 2020, 10, 5672−5680